Pergamon

Geochimica et Cosmochimica Acta, Vol. 62, No. 18, pp. 3109–3116, 1998

0016-7037/98 $19.00 + .00

PII S0016-7037(98)00213-0

Non-Rayleigh oxygen isotope fractionation by mineral evaporation: Theory and experiments in the system SiO_2

EDWARD D. YOUNG,[1,*] HIROKO NAGAHARA,[2] BJORN O. MYSEN,[3] and DENIS MARC AUDET[1]

[1]Department of Earth Sciences, University of Oxford, Oxford OX1 3PR, UK
[2]Geological Institute, University of Tokyo, 7-3-1 Hongo, Tokyo 113, Japan
[3]Geophysical Laboratory, Carnegie Institution of Washington, Washington D.C., 20015

Abstract—Experiments demonstrate that partial evaporation of solid silica at 1600–1700°C and low pressure (10^{-9} bar) results in enrichment of $^{18}O/^{16}O$ and $^{17}O/^{16}O$ in solid products. Evaporative residues formed in H_2 or N_2 gas at higher pressures ($>10^{-5}$ bar) exhibit limited or negligible heavy isotope enrichment. The degree of enrichment is controlled by kinetic fractionation at the ablating grain surfaces, the rate of sublimation, and the efficacy of oxygen self diffusion in the solid. Observed isotopic effects are consistent with numerical simulations, confirming that vaporization of solid silicate and oxide minerals is a viable cause for non-Rayleigh fractionation of ^{16}O, ^{17}O, and ^{18}O. Experiment and theory suggest that partial melting during evaporation is not required *a priori* to explain mass-dependent variations in oxygen isotope ratios in primitive meteoritical materials. Experimental determinations of the rates of ablation of appropriate minerals are required to evaluate the meteoritical data.

1. INTRODUCTION

The precursor material for planets and meteorites was silicate, oxide, metal, and sulfide dust. These protoplanetary mineral grains were subjected to large temperature fluctuations as they migrated through the early solar nebula (Chou et al., 1976; Hashimoto et al., 1979; Morfill, 1983; Morfill and Völk, 1984; Boss, 1995). Hydrodynamic calculations suggest that evaporation of solid mineral dust was a likely result of either turbulent transport through a hot central region of the protoplanetary disk (Morfill, 1983) or heating at midplane heliocentric distances out to 2.5 AU during an inward spiral toward the nascent sun (Boss, 1993). Transient heating by shock waves has also been proposed (Clayton and Jin, 1995).

Results of previous experimental studies imply that melting must occur for appreciable fractionation among the isotopes of Si, Mg, and O to be preserved in evaporative residues (Molini-Velsko et al., 1987; Esat et al., 1986; Davis et al., 1990). For example, solid residues of molten forsterite volatilization record large (tens of ‰ amu^{-1}) kinetic isotope fractionations for these elements (Davis et al., 1990). The same study demonstrated that partial evaporation of solid forsterite produces shifts of $\leq$1‰ amu^{-1} for Si, Mg, and O after nearly 80% weight loss.

We report here results of experiments demonstrating that melting is not required *a priori* for oxygen isotope fractionation to be recorded in the residues of partial evaporation. SiO_2 was chosen for study because evaporation in this system is well understood (Mysen and Kushiro, 1988; Hashimoto, 1990). Heavy isotope enrichment in SiO_2 subjected to partial evaporation is explained by pure kinetic mass-dependent fractionation at the surfaces of the subliming grains combined with diffusive transport within grain interiors. The process is quantified by two parameters, the kinetic isotope fractionation factor, and the ablative-diffusive Peclet number. Previously published results of laboratory experiments for both melts and solids are also successfully modeled using this computational approach.

*Author to whom correspondence should be addressed (ed.young@earth.ox.ac.uk).

2. EXPERIMENTAL PROCEDURES

Evaporation was carried out in a high-vacuum furnace described by Mysen et al. (1985) and Mysen and Kushiro (1988). The furnace assembly consisted of a Mo-wound alumina tube measuring 5 cm in length and 1 cm in diameter (id) situated coaxially within a cylindrical stainless steel vacuum chamber. Temperatures along the tube were measured with W-$W_{74}Re_{26}$ thermocouples interfaced with programmable temperature controllers. Uncertainty in temperature measurements of the hot zone of the furnace is approximately ±10°C or better. High vacuum was provided by a turbomolecular pump. Background pressure was approximately 1×10^{-10} bar as measured with an ionization gauge. Desired steady-state pressures of H_2 and N_2 gas were obtained by bleeding these gases into the chamber through needle valves during pumping.

Graphite Knudsen cells were used to suspend samples in the hot-zone of the furnace. The cells were 4 mm deep by 3 mm or 1.5 mm diameter with two 0.5 mm holes positioned near the top. Open-system evaporation was accomplished by loading samples into the cells without lids, permitting rapid removal of evolved gases. Weight loss was determined by weighing samples and cells before and after runs.

Two starting materials were used. Material 1 consisted of powder obtained by grinding a single crystal of α-quartz. Material 2 was made by sintering quartz powder at 1600°C for two days. Raman microprobe spectroscopy of polished sections reveals that the sintered grains were composed of quartz interiors with mantles of cristobalite. Grains comprising both SiO_2 samples varied from 120 μm to 300 μm in diameter with an approximate mean of 200 μm. Samples consisted of between 3 and 13 mg of SiO_2 powder at the start of each experiment.

Oxygen isotope ratios of starting materials and run products were measured by laser-heating fluorination and gas-source ratio mass spectrometry. Oxygen was extracted by heating with a 20 Watt CO_2 laser in the presence of F_2 gas. Purified F_2 was delivered to the samples by heating $K_2NiF_6 \cdot KF$ powder to greater than 250°C. The laser was operated at 5–6 W with 0.1 kHz beam modulation. Liberated O_2 was trapped onto molecular sieve 13× at −196°C. Ubiquitous trace amounts of NF_3 were removed through a second cryogenic transfer of analyte O_2 from the first 13× mol sieve at −130°C to a second molecular sieve at −196°C for 10 min (Clayton, pers. commun.; Thiemens and Meagher, 1984). Elimination of NF_3 removes mass interference of the $^{17}O^{16}O$ isotopomer by NF. Simultaneous measure-

Table 1. Results of SiO_2 evaporation experiments

T (C)	Gas	P (bar)	[1]$\delta^{18}O$	[2]$\delta^{17}O$	% Wt loss	Time (min)	[3]r^*
[4]1600	—	6.0×10^{-10}	3.0	1.3	61.5	750	73
[4]1600	—	6.0×10^{-10}	6.6	3.2	80.1	2000	58
[4]1600	—	6.0×10^{-10}	6.0	3.0	79.8	1200	59
[4]1600	—	6.0×10^{-10}	0.3	0.0	36.1	600	86
[4]1600	—	6.0×10^{-10}	4.5	2.2	64.4	900	71
[4]1600	—	6.0×10^{-10}	0.1	−0.4	31.8	441	88
[4]1600	—	6.0×10^{-10}	6.0	3.1	71.1	1650	66
[4]1600	—	6.0×10^{-10}	7.3	3.4	72.7	1350	65
[4]1600	—	6.0×10^{-10}	−1.1	−0.9	25.6	150	91
[4]1600	—	6.0×10^{-10}	0.5	0.5	31.8	300	88
[4]1600	—	6.0×10^{-10}	4.1	1.9	31.4	360	88
[4]1600	—	6.0×10^{-10}	5.9	2.8	54.5	1100	77
[4]1600	—	6.0×10^{-10}	4.7	1.7	46.3	720	81
[4]1600	—	6.0×10^{-10}	8.5	—	86.0	1440	52
[4]1600	—	6.0×10^{-10}	0.2	0.1	25.6	60	91
[5]1600	—	1.1×10^{-9}	1.2	—	2.3	20	99
[5]1600	—	6.6×10^{-9}	1.2	—	7.2	60	98
[5]1600	—	1.2×10^{-9}	1.4	—	11.1	120	96
[5]1600	—	1.1×10^{-9}	1.9	—	25.6	240	91
[5]1600	—	7.9×10^{-10}	1.6	—	22.2	420	92
[5]1600	—	4.0×10^{-10}	3.4	—	47.8	900	81
[5]1700	—	1.3×10^{-9}	1.1	—	2.7	120	99
[5]1700	—	6.6×10^{-9}	3.2	—	48.7	240	80
[4]1600	N_2	2.7×10^{-4}	0.3	−0.4	32.0	300	88
[4]1600	N_2	2.7×10^{-4}	2.9	1.2	60.4	525	73
[4]1600	N_2	2.7×10^{-4}	−1.1	−1.2	12.7	75	96
[4]1600	N_2	2.7×10^{-4}	0.6	0.2	46.8	450	81
[4]1600	N_2	2.7×10^{-4}	1.3	0.5	81.8	825	57
[4]1600	N_2	2.7×10^{-4}	2.8	1.5	42.2	225	83
[4]1600	N_2	2.7×10^{-4}	1.3	0.6	63.3	675	72
[5]1600	H_2	2.7×10^{-5}	1.9	—	21.3	30	92
[5]1600	H_2	2.7×10^{-5}	2.0	—	46.5	60	81
[5]1600	H_2	2.7×10^{-5}	1.3	—	69.8	120	67
[5]1600	H_2	2.7×10^{-7}	1.9	—	19.0	120	93
[5]1600	H_2	2.7×10^{-7}	1.7	—	38.9	360	85
[5]1600	H_2	2.7×10^{-7}	2.8	—	48.9	810	80
[5]1600	H_2	2.7×10^{-7}	3.0	—	69.5	1440	67

[1]$(({}^{18}O/{}^{16}O)/({}^{18}O/{}^{16}O)^\circ - 1) \times 10^3$ where ° is the initial ratio.
[2]$(({}^{17}O/{}^{16}O)/({}^{17}O/{}^{16}O)^\circ - 1) \times 10^3$ where ° is the initial ratio.
[3]Calculated average grain radius (μm) of powder based on an initial radius of 100 μm.
[4]Starting material 2 described in the text.
[5]Starting material 1 described in the text.

ments of $^{18}O/^{16}O$ and $^{17}O/^{16}O$ were made on a Nuclide triple-collector mass spectrometer equipped with a microvolume trap for analysis of small O_2 gas samples. Measurements of $^{18}O/^{16}O$ alone were made using a Finnigan MAT 252 mass spectrometer. Several samples were analyzed for $^{18}O/^{16}O$ using CO_2 gas as analyte following conversion of O_2 to CO_2 over hot graphite. External precision of the isotope ratio determinations is ±0.1 and ±0.3 per mil for $\delta^{18}O$ and $\delta^{17}O$, respectively. Accuracy is ±0.1 per mil (Young and Rumble, 1993).

Run products exhibited reductions in grain size but sintering made quantifying this effect difficult. In lieu of accurate grain-size statistics, the weight loss of each run was converted to an effective mean grain radius r^* with the expression $x = 1 - (r^*)^3/(r^\circ)^3$ where x is the fractional weight loss, and r° is the average grain size of the starting material (100 μm).

3. RESULTS

We report on evaporation of SiO_2 carried out under four different experimental conditions: (1) open-system to vacuum (free evaporation), (2) open-system with an imposed dynamic steady-state H_2 pressure of 2.7×10^{-7} bar, (3) open-system with a dynamic steady-state H_2 pressure of 2.7×10^{-5} bar, and (4) open-system with a dynamic steady-state N_2 pressure of 2.7×10^{-4} bar. Results are summarized in Table 1.

Evaporation was slowest during free evaporation. Higher pressures resulted in more rapid weight loss (Fig. 1), although any difference that might have obtained between the rates of free evaporation (10^{-9} bar) and evaporation in 2.7×10^{-7} bar H_2 could not be distinguished. Variation of effective mean grain radii with time was essentially linear for all conditions (e.g., Fig. 2). Nagahara et al. (1993) raised the possibility that enhancement of SiO_2 evaporation rate might be the result of amorphization at grain surfaces. Grains record no evidence for reaction between residual SiO_2 and H_2 within the ≃10 μm resolution of laser Raman microprobe spectroscopy (Fig. 3).

Residues of free evaporation are substantially enriched in ^{18}O and ^{17}O relative to ^{16}O in mass-dependent fashion (Fig. 2, Table 1). Enrichments are also evident in the products of evaporation in the presence of an ambient H_2 pressure of 2.7

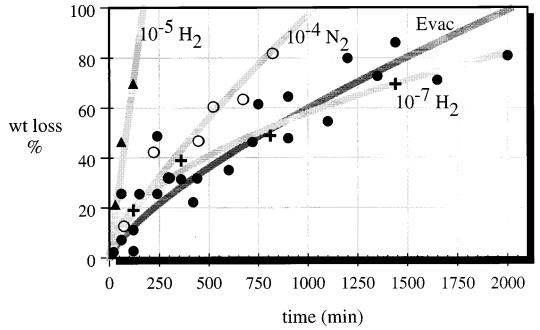

Fig. 1. Plot of percent weight loss vs. time (minutes) for all SiO_2 evaporation experiments. Solid dots are free-evaporation (Evac) data, open dots are 2.7×10^{-4} bar N_2 data, crosses are 2.7×10^{-7} bar H_2 data, and triangles are 2.7×10^{-5} bar H_2 data. Dark grey curve is best-fit to free-evaporation data. Light grey curves are best fits to labelled data.

$\times 10^{-7}$ bar. Higher pressures of both H_2 and N_2 exhibit negligible increases in $\delta^{18}O$ and $\delta^{17}O$ (Fig. 4). The data define a negative correlation between rate of evaporation and magnitude of heavy isotope enrichment.

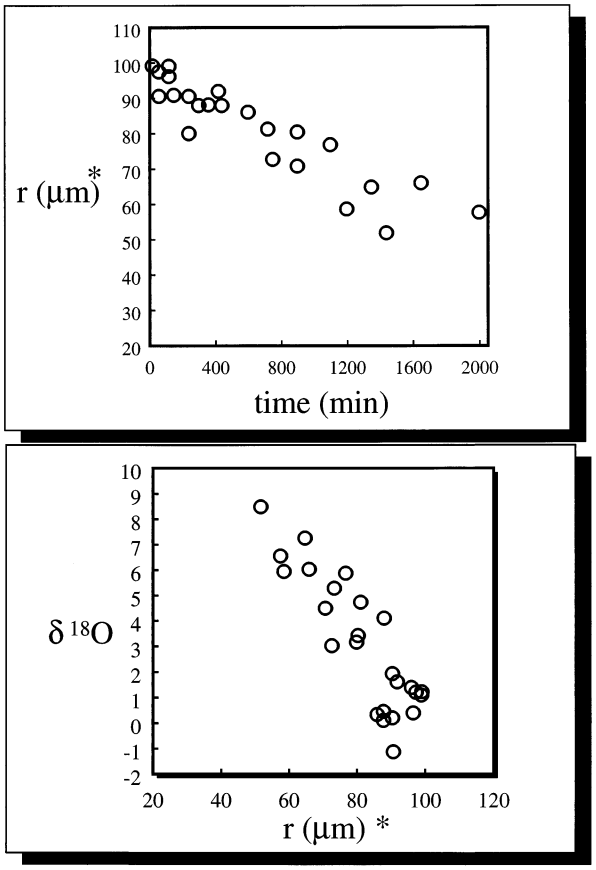

Fig. 2. Plots of effective average grain radius r^* based on an initial radius of 100 μm vs. time (top) and $\delta^{18}O$ (bottom) for free-evaporation SiO_2 residues.

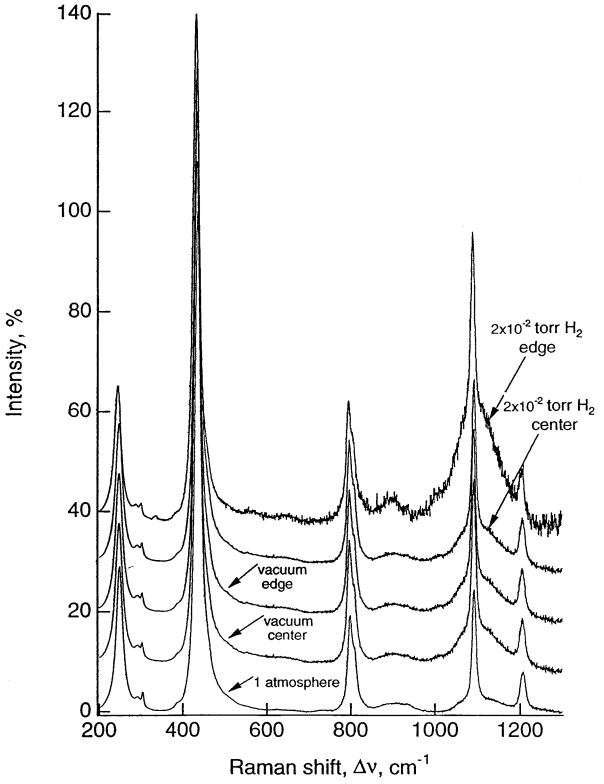

Fig. 3. Normalized micro-Raman spectra of SiO_2 grains evaporated at 1600°C in C cells. Shown are the starting material (one atmosphere), the center of a grain after substantial evaporation in vacuum (vacuum center), the edge (within several μm) of the grain evaporated in vacuum (vacuum edge), the center of a grain evaporated in 2.7×10^{-5} bar H_2 (center), and the edge (within several μm) of the grain evaporated in H_2 gas (edge). Fuzziness and broadening in the top spectrum is an artifact of interaction between the incident laser and the mounting medium.

4. DISCUSSION

4.1. Physical Model

The importance of volume diffusion as a limiting factor for bulk isotope exchange between condensed phases and vapor has been noted previously (Davis et al., 1990) as has the contrast between diffusion-limited isotope fractionation and Rayleigh fractionation (Esat, 1996; Nagahara and Ozawa, 1997). Although approximations have been put forth (e.g., Wang et al., 1993), a fully quantitative treatment of non-Rayleigh, or diffusion-limited, fractionation has been lacking. Results of such a treatment are presented here to explain the oxygen isotope data collected in the present study as well as light stable isotope data from other published experimental results.

We have obtained both numerical and asymptotic analytical solutions to the problem of isotopic fractionation at the moving surface of a shrinking (or growing) sphere coupled with diffusional transport within the sphere. Solutions to this moving-boundary problem have not been published previously, and a complete description is to be presented elsewhere. Below we

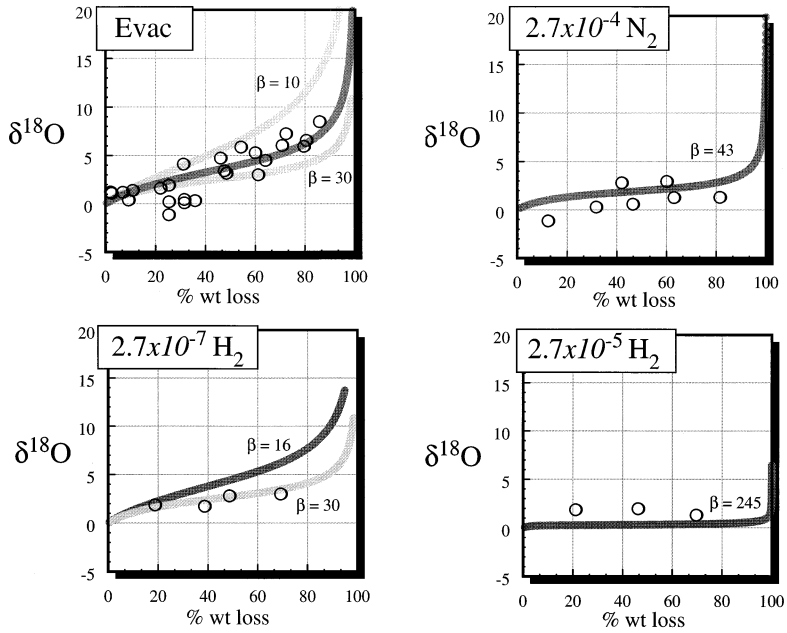

Fig. 4. Plots of $\delta^{18}O$ against percent weight loss for SiO_2 evaporated in vacuum (EVAC) and in dynamic steady-state pressures of the indicated gas. Dark grey lines are model curves based on an α of 0.977 and β corresponding to measured rates of evaporation, average radius, and an oxygen diffusivity of 1.9×10^{-11} cm$^2 \cdot$ sec^{-1}. Additional model curves are for specified values of β.

describe the equations comprising the model and pertinent numerical solutions.

SiO_2 evaporation is likely to have occurred by one of two different reactions

$$SiO_2(s) \rightarrow SiO(v) + \frac{1}{2}O_2(v) \quad (1)$$

$$SiO_2(s) \rightarrow SiO_2(v) \quad (2)$$

Evaporation by reaction 1 would produce the thermodynamically stable gaseous species but would proceed with a significant kinetic barrier (Hashimoto, 1990). Reaction 2 would yield unstable gaseous SiO_2 but is not hampered by a kinetic barrier (Hashimoto, 1990). We show below that oxygen isotope fractionation is unlikely to be different for the two reactions.

Evaporation gives rise to mass-dependent isotope fractionation. The ratio of the rate of sublimation of the heavy isotope to that of the lighter isotope is parameterized by the fractionation factor α

$$\alpha = \frac{\left(\frac{^{18}O}{^{16}O}\right)_v}{\left(\frac{^{18}O}{^{16}O}\right)_s} = \frac{\left(\frac{c^{18_O}}{c^{16_O}}\right)_v}{\left(\frac{c^{18_O}}{c^{16_O}}\right)_s} \quad (3)$$

where c^{18_O} and c^{16_O} are the concentrations (mol cm^{-3}) of ^{18}O and ^{16}O for the solid (s) and vapor (v) phases. Alteration of the concentrations of ^{18}O and ^{16}O at grain surfaces drives diffusion.

One method for estimating α is to assume that the rate limiting step is the average velocity of the volatilizing molecules as they leave the surface of the evaporating mineral grain. In this case the mass dependence of vapor pressure dominates, and the kinetic theory of gases yields

$$\alpha = \sqrt{\frac{m}{m'}} \quad (4)$$

where m is the mass of the evaporating species and $'$ denotes the heavy (rare) isotopomer of that species. Nonclassical effects are excluded in reaction 4 as they have a negligible influence on kinetic fractionation at high temperatures (i.e., above 1000 K). In the case of reaction 2, the dominant fractionating isotopomers are $^{28}Si^{16}O^{16}O$ and $^{28}Si^{18}O^{16}O$, yielding a value of 0.984 for α using Eq. 4 (the rare silicon isotopes ^{29}Si and ^{30}Si contribute less than 0.0001 to α and are safely ignored in this calculation).

The kinetic barrier to progress of reaction 1 can be regarded in the context of transition state theory as resulting from the energy required to form the activated complex SiO_2^*

$$SiO_2(s) \rightarrow SiO_2^* \rightarrow SiO(v) + \frac{1}{2}O_2(v) \quad (5)$$

The relative rates of translation of the activated complex away from the mineral to form SiO and O_2 vapor will depend on the mass of the complex. The value for α for reaction 1 is, therefore, the same as that for reaction 2.

Another method for estimating α is to consider that the rate-controlling step during evaporation is the breaking of Si-O bonds in the solid SiO_2 structure rather than the mean velocity of the volatilizing molecules. The rate constant κ (sec^{-1}) of bond rupture can be described by the Arrhenius expression

$$\kappa = \nu \exp\left(\frac{-E_a}{kT}\right) \tag{6}$$

where k is Boltzmann's constant, and T is temperature. Slater (1948) identified ν with the frequency of reaction attempts and the activation energy E_a with the kinetic barrier between the zero-point energy and the energy of the activated state in which bonds along the reaction coordinate are at critical extension. In the high temperature limit applicable in this study, differences in nonclassical effects such as zero-point energies upon isotope substitution are small in comparison with kT and can be ignored. The isotope fractionation factor is then

$$\alpha = \frac{\kappa'}{\kappa} \simeq \frac{\nu'}{\nu} \tag{7}$$

Bigeleisen and Wolfsberg (1958) showed that ν can be interpreted as the frequency of vibration in the direction of bond rupture (the reaction coordinate). In the absence of an atomic dynamical model for the evaporation process, α must be estimated from measured shifts in vibrational modes with substitution of ^{18}O for ^{16}O. Frequency shifts in solid SiO_2 can be used for this purpose because the rate-limiting step is likely to be associated with the first Si-O rupture when the structure is still that of the reactant solid. High-frequency Si-O stretches along Si-O-Si linkages offer the greatest opportunity for bond rupture and isotopic shifts for these modes in quartz range from 0.956 to 0.966 (Sato and McMillan, 1987), suggesting that α may have been as low as 0.96.

For a spherical grain, diffusion of ^{18}O driven by a change in c^{18_O} at the surface is described by the equation

$$\frac{\partial c^{18_O}}{\partial t} = D\left(\frac{\partial^2 c^{18_O}}{\partial r^2} + \frac{2}{r}\frac{\partial c^{18_O}}{\partial r}\right),\ 0 < r < s(t) \tag{8}$$

where D is the diffusivity of oxygen ($cm^2\ sec^{-1}$), r is the radial distance from the center of the sphere, and $s(t)$ is the time-dependent radial position of the sphere surface.

Mass balance obtains at the surface of the spherical grain expressed as

$$\mathbf{J}^{^{18}O}_{evap} = \mathbf{J}^{^{18}O}_{diff} - \mathbf{J}^{^{18}O}_{ablt} \tag{9}$$

$\mathbf{J}^{^{18}O}_{evap}$ in (9) is the evaporative flux of ^{18}O toward the vapor side of the interface, $\mathbf{J}^{^{18}O}_{diff}$ is the diffusive flux of ^{18}O in the solid, and $\mathbf{J}^{^{18}O}_{ablt}$ is the ablative flux associated with motion of the interface. Fluxes are defined in terms of rate of ablation, $\dot{s}$ (ds/dt, positive in the direction of increasing r), and diffusivity

$$\mathbf{J}^{^{18}O}_{ablt} = c^{^{18}O}_{s}\,\dot{s},\ \mathbf{J}^{^{18}O}_{evap} = -c^{^{18}O}_{v}\,\dot{s},\ \mathbf{J}^{^{18}O}_{diff} = -D\frac{\partial c_s^{^{18_O}}}{\partial r}\bigg|_{r=s(t)} \tag{10}$$

Substitution of 10 into 9 yields the boundary condition prescribed by mass balance at the surface of the subliming spherical grain

$$D\frac{\partial c^{^{18}O}_{s}}{\partial r}\bigg|_{r=s(t)} = c^{^{18}O}_{s}(\alpha - 1)\dot{s} \tag{11}$$

Equation 11 includes the approximation

$$\alpha = \frac{\left(\frac{c^{18_O}}{c^{16_O}}\right)_v}{\left(\frac{c^{18_O}}{c^{16_O}}\right)_s} \approx \frac{(c^{18_O})_v}{(c^{18_O})_s} \tag{12}$$

since ^{16}O approximates total O. The error incurred by 12 is below detection levels.

The problem is made more tractable by converting to nondimensional variables where ° signifies the initial value of a superscripted parameter

$$c' = \frac{c^{18_O}}{c^{18_{O^\circ}}},\ r' = \frac{r}{s^\circ},\ s' = \frac{s}{s^\circ},\ t' = \frac{tD}{(s^\circ)^2} \tag{13}$$

and by applying two transformations of coordinates

$$u = r'c' \quad \text{and} \quad R = \frac{r'}{s'} \tag{14}$$

The first transformation from c' to u is usual for spherical problems. The second is attributed to Landau (1950) and allows the moving boundary to be accommodated by scaling dimensionless radial distance r' to the time-dependent dimensionless position of the surface s'.

After substitution of scaled variables and transforming to coordinates u and R, the diffusion Eq. 8 becomes

$$s'^2\frac{\partial u}{\partial t'} = \frac{\partial^2 u}{\partial R^2} - \beta R s'\frac{\partial u}{\partial R},\ 0 < R < 1 \tag{15}$$

and the surface boundary condition 11 becomes

$$\frac{\partial u}{\partial R}\bigg|_{R=1} = u(1 - \beta s'(\alpha - 1)) \tag{16}$$

where

$$\beta = -\dot{s}' = -s^\circ\frac{\dot{s}}{D} \tag{17}$$

Parameter β, the dimensionless rate of surface migration, is identified as the Peclet number for ablative and diffusive transport.

4.2. SiO_2

Equations 15 and 16 together with the boundary condition $u = 0$ at $R = 0$ were solved numerically using fully implicit finite difference with second-order accuracy in time. Radial profiles of $\delta^{18}O$, representing individual grains of a bulk SiO_2 sample, were integrated to obtain bulk $\delta^{18}O$ values at different fractional weight losses for comparison with the experimental data. The free-evaporation SiO_2 data were fit by adjusting β at a prescribed α. The latter was varied between ~0.960, representing rate control by the frequency of Si-O stretching, and ~0.984, representing the classical vapor pressure effect as described above. The best-fit beta for $\alpha = 0.960$ is 37 while for $\alpha = 0.984$ it is 15.

An intermediate α value of 0.977 is consistent with previous

kinetic calculations presented by Davis et al. (1990) and is used here to construct curves of constant β in Fig. 4. Curves representing β between 10 and 30 envelope most of the free-evaporation data at this α. The best fit is obtained with $\beta = 20$ (Fig. 4). The range in β about the best fit is consistent with the spread in starting material grain size. The necessary simplifying assumption in the calculations that the ablating grains were spherical contributes to scatter about the model curves. Scatter at low weight loss extending below zero in $\delta^{18}O$ is larger than analytical uncertainties and requires that some of the range in β is also the result of inhomogeneity in the initial isotopic compositions of the starting materials.

The best-fit β for $\alpha = 0.977$, together with the average radius of the starting material (100 μm) and the measured rate of evaporation (3.75×10^{-8} cm/sec), defines an oxygen diffusivity of 1.9×10^{-11} cm$^2 \cdot$ sec^{-1}. This value for the diffusivity is approximately ten times larger than the experimental value determined by quartz-CO_2 exchange at 100 bar (Sharp et al., 1991) and a factor of 100 larger than the value obtained by quartz-O_2 exchange at subatmospheric pressures (Dennis, 1984). Varying α within reasonable limits has little affect on the extracted value for D. The range in expected values for α (from 0.960 to 0.984) produces a corresponding spread in best-fit β values of 22 and thus a factor of 2 variability in D. The factor of 2 is small in comparison with the discrepancies in experimentally-determined diffusivities. We note that extrapolation of more than 400°C is required to compare the quartz diffusivities with our cristobalite sublimation data, and this may be partly to blame.

If the physical model described above is applicable to open-system evaporation in general, one expects that the kinetic α and average grain size should yield β curves that fit all of the experimental data when the diffusivity defined by the free-evaporation data is combined with the different measured rates of evaporation. Curves obtained in this way are shown in dark grey in Fig. 4. Satisfactory fits are obtained with the possible exception of the 2.7×10^{-7} H_2 data. In the latter case, the expected β is 16 while a value of 30 best fits the data. The best-fit value is outside the range of 5–25 expected on the basis of the variable grain size of the starting material. All else equal, a D value of 1.0×10^{-11} cm$^2 \cdot$ sec^{-1} would be required to obtain a β of 30 and thus fit the low-pressure H_2 data. The discrepancy between required diffusivities is similar for all α within the expected range of values. In view of the small number of H_2 runs, the difference between 1.0×10^{-11} and 1.9×10^{-11} cm$^2 \cdot$ sec^{-1} for D is considered to be well within the uncertainties of these experiments.

An apparent increase in best-fit β for the low-pressure H_2 runs could result from an increase in α relative to the free evaporation experiments. Larger α would not be inconsistent with the higher-pressure H_2 data because of the negligible isotope shifts exhibited by the latter. Variable α would be difficult to explain in the context of Si-O vibrational control over the relative rates of evaporation, especially as there is no evidence for reaction between solid SiO_2 and H_2 in these experiments (Fig. 3) that might modify the mineral structure during evaporation. An increase in α would more easily be explained by evaporation of molecular species heavier than the products of free evaporation. Because the obvious products of reaction between SiO_2 and H_2, SiO and H_2O, would shift α to lower rather than higher values, we consider a shift in α because of the presence of hydrogen gas unlikely. Larger α values could also result from back reaction between vapor and solid if the system were able to move toward a state of equilibrium. However, significant deviation from kinetic fractionation is also unlikely because of the dynamic flow conditions and low pressures that obtained during these experiments (cf. Nagahara and Ozawa, 1996).

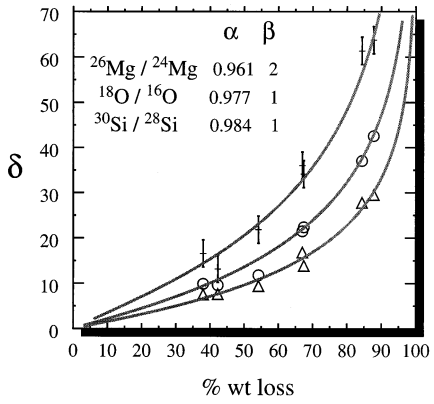

Fig. 5. Comparison of experimental data for molten forsterite from Davis et al. (1990) (data points) with model calculations for diffusion-limited kinetic isotope fractionation (curves). Plot shows bulk $\delta^{18}O$ (circles), $\delta^{26}Mg$ (crosses with error bars), and $\delta^{30}Si$ (triangles) vs. percent weight loss following evaporation from 1900 to 2050°C. Values for α and β used to generate curves are indicated.

4.3. Mg_2SiO_4

Non-Rayleigh kinetic fractionation can be used to explain the silicon, magnesium, and oxygen isotope effects of molten forsterite evaporation reported by Davis et al. (1990). Data for $\delta^{30}Si$, $\delta^{26}Mg$, and $\delta^{18}O$ are fit with purely kinetic α values of 0.984, 0.961, and 0.977 (see Davis et al. (1991) for derivation of α values) and β of 1, 2, and 1, respectively (Fig. 5). Whereas Davis et al. (1991) found that these kinetic fractionation factors could not be used to fit their experimental data using a Rayleigh fractionation model, Fig. 5 shows that they can explain the observed fractionation when diffusion in the melt is considered. Best-fit values for β correspond to O and Si diffusivities of 5.0×10^{-5} cm$^2 \cdot$ sec^{-1} and an Mg diffusivity of 2.5×10^{-5} cm$^2 \cdot$ sec^{-1} when combined with the rate of evaporation (1.69×10^{-4} cm/sec) and the approximate diameter of the molten charges as indicated by Davis et al. (1991) and references therein (diameter taken to be 0.3 cm based on the volume of sample and the assumption that the charge was in the form of a sphere upon melting).

The plausibility of the physical model used to explain the molten forsterite isotope data depends in part upon the reasonableness of the derived diffusivities. Eyring's equation:

$$D = \frac{kT}{\eta\lambda} \tag{18}$$

is used to estimate expected diffusivities where k is Boltzmann's constant, T is temperature, η is viscosity, and λ the effective jump distance for the migrating species. Data presented by Wasserman et al. (1993) suggest λ values of 0.376 nm for Mg and 0.310 for Si, representing twice the coordination radii for Mg-O and Si-O in the melt phase, respectively. A λ of 0.28 nm is appropriate for O based on its atomic diameter. At the temperature of the evaporation experiments an appropriate viscosity is 0.0267 Pa · sec assuming the melt was composed of 34.9% SiO_2 and 65.1% MgO by weight (Urbain et al., 1982). With these values the calculated diffusivities are 3.2×10^{-5} for Mg, 3.9×10^{-5} for Si, and 4.3×10^{-5} $cm^2 \cdot sec^{-1}$ for O. In view of the uncertainties, the similarity between Eyring diffusivities and diffusivities required by the modeling is taken as evidence that pure kinetic fractionation at the surface of the molten forsterite combined with self diffusion of Mg, Si, and O adequately explains the observed bulk isotopic shifts attending evaporation.

The geometry of the experiments on solid forsterite is unclear from the literature and so detailed modeling was not attempted. However, Nagahara and Ozawa (1996) report a free-evaporation rate of 3.1×10^{-7} cm/sec for forsterite, a factor of 10 larger than the measured SiO_2 value. When combined with the rate of oxygen self diffusion in forsterite (e.g., Geral and Jaoul, 1989), the rate of forsterite evaporation requires that β was sufficiently high to all but preclude transport of the surface kinetic isotope enrichment into the solid mineral. Thus the lack of enrichment observed by Davis et al. is to be expected given the high rate of forsterite evaporation.

5. CONCLUSION

Evaporation is expected to lead to kinetic isotope fractionation. Experiments with SiO_2 demonstrate that melting is not required *a priori* for preservation of oxygen isotopic evidence of evaporation despite the low diffusivities of O in solid silicate relative to melt. Rather, the extent of bulk isotopic fractionation depends on the rate of evaporation, controlled in part by total ambient pressure, as well as oxygen diffusivity.

Agreement between experiments and theoretical calculations in the SiO_2 and Mg_2SiO_4 systems indicates that the isotopic effects of evaporation can be understood in terms of pure kinetic fractionation at surfaces of condensed phases combined with the relative rates of ablation and diffusive transport within condensed phase interiors. Two parameters are sufficient to quantify the process, the kinetic fractionation factor and the ablative-diffusive Peclet number.

Solid SiO_2 evaporates more slowly than solid Mg_2SiO_4 by a factor of 10. This difference in rate of sublimation proves to be the difference between preservation of the isotopic record of evaporation and obliteration of that record. Interpretation of light stable isotope ratios in primitive meteoritical materials thus requires knowledge of rates of evaporation as well as self diffusion for the pertinent elements and phases. Such knowledge will have to come from further experiments.

Acknowledgments—Useful comments by two anonymous reviewers of the original manuscript are gratefully acknowledged. The first author wishes to thank Dr. Douglas Rumble III for use of his stable isotope laboratory and the Carnegie Institution of Washington's Geophysical Laboratory for support as a postdoctoral fellow during the experimental phase of this study.

REFERENCES

Bigeleisen J. and Wolfsberg M. (1958) Theoretical and experimental aspects of isotope effects in chemical kinetics. *Adv. Chem. Phys.* **1,** 15–74.

Boss A. (1995) Timing is everything. *Nature* **375,** 13–14.

Boss A. (1993) Evolution of the solar nebula II. Thermal structure during nebula formation. *Astrophys. J.* **417,** 351–367.

Chou C., Baedecker P. A., and Wasson J. T. (1976) Allende inclusions: Volatile-element distribution and evidence for incomplete volatilization of presolar solids. *Geochim. Cosmochim. Acta* **40,** 85–94.

Clayton D. D. and Jin L. (1995) Origin of CAIs and of their high aluminum-26 concentrations. *Meteoritics* **30,** 499–500.

Davis A. M., Hashimoto A., Clayton R. N., and Mayeda T. K. (1990) Isotope mass fractionation during evaporation of Mg_2SiO_4. *Nature* **347,** 655–658.

Dennis P. F. (1984) Oxygen self difusion in quartz. *NERC Publ. D* **25,** 260–265.

Esat T. M. (1996) Comment on "Potassium isotope cosmochemistry: Genetic implications of volatile element depletion" by Munir Humayun and R. N. Clayton. *Geochim. Cosmochim. Acta* **60,** 3755–3758.

Esat T. M., Spear R. H., and Taylor S. R. (1986) Isotope anomalies induced in laboratory distillation. *Nature* **319,** 576–578.

Geral O. and Jaoul O. (1989) Oxygen diffusion in San Carlos olivine. *J. Geophys. Res.* **94,** 4119–4128.

Hashimoto A. (1990) Evaporation kinetics of forsterite and implications for the early solar nebula. *Nature* **347,** 53–55.

Hashimoto A., Kumazawa M., and Onuma N. (1979) Evaporation metamorphism of primitive dust material in the early solar nebula. *Earth Planet. Sci. Lett.* **43,** 13–21.

Landau H. G. (1950) Heat conduction in a melting solid. *Q. Appl. Math* **8,** 81–94.

Molini-Velsko C., Mayeda T. K., and Clayton R. N. (1987) Silicon isotope systematics during distillation. *Lunar Planet. Sci.* **XVIII,** 657–658.

Morfill G. E. (1983) Some cosmochemical consequences of a turbulent protoplanetary cloud. *Icarus* **53,** 41–55.

Morfill G. E. and Völk H. J. (1984) Transport of dust and vapor and chemical fractionation in the early protosolar cloud. *Astrophys. J.* **287,** 371–395.

Mysen B. O. and Kushiro I. (1988) Condensation, evaporation, melting, and crystallization in the primitive solar nebula: Experimental data in the system $MgO\text{-}SiO_2\text{-}H_2$ to 1.0×10^{-9} bar and 1870°C with variable oxygen fugacity. *Amer. Mineral.* **73,** 1–19.

Mysen B. O., Virgo D., and Kushiro I. (1985) Experimental studies of condensation processes in silicate materials at low pressures and high temperatures. I. Phase equilibria in the system $CaMgSi_2O_6\text{-}H_2$ in the temperature range 1200–1500°C and the pressure range (P_{H2}) 10^{-6} to 10^{-9} bar. *Earth Planet. Sci. Lett.* **75,** 139–145.

Nagahara H. and Ozawa K. (1997) Isotopic fractionation as a probe of evaporation processes in stellar environments. *Lunar Planet. Sci.* **XXVIII,** 997–998.

Nagahara H. and Ozawa K. (1996) Evaporation of forsterite in H_2 gas. *Geochim. Cosmochim. Acta* **60,** 1445–1459.

Nagahara H., Young E. D., Hoering T. C., and Mysen B. O. (1993) Oxygen isotopic fractionation during evaporation of SiO_2 in vacuum and in H_2 gas. *Meteoritics* **28,** 406–407.

Sato R. K. and McMillan P. F. (1987) An infrared and Raman study of the isotopic species of α-quartz. *J. Phys. Chem.* **91,** 3494–3498.

Sharp Z. D., Giletti B. J., and Yoder H. S. Jr. (1991) Oxygen diffusion rates in quartz exchanged with CO_2. *Earth Planet. Sci. Lett.* **107,** 339–348.

Slater N. B. (1948) Aspects of a theory of unimolecular reaction rates. *Proc. Royal Soc. A* **194,** 112–131.

Thiemens M. H. and Meagher D. (1984) Cryogenic separation of nitrogen and oxygen in air for determination of ratios by mass spectrometry. *Anal. Chem.* **56,** 201–203.

Urbain G., Bottinga Y., and Richet P. (1982) Viscosity of liquid silica,

silicates and alumino-silicates. *Geochim. Cosmochim. Acta* **46,** 1061–1072.

Wang J., Davis A. M., Hashimoto A., and Clayton R. N. (1993) Diffusion-controlled magnesium isotopic fractionation of a single crystal forsterite evaporated from the solid state. *Lunar Planet. Sci.* **XXIV,** 1479–1480.

Wasserman E. A., Yuen D. A., and Rustad J. R. (1993) Molecular dynamics study of the transport properties of perovskite melts under high temperature and pressure conditions. *Earth Planet. Sci. Lett.* **114,** 373–384.

Young E. D. and Rumble D., III (1993) The origin of correlated variations in $^{18}O/^{16}O$ and elemental concentrations in metamorphic garnet from southeastern Vermont, USA. *Geochim. Cosmochim. Acta* **57,** 2585–2597.